Highly directional emission from ultra-small photonic crystal resonators

Se-Heon Kim[a], Yong-Hee Lee[b], Jingqing Huang[a], and Axel Scherer[a]

[a] Department of Electrical Engineering, California Institute of Technology, Pasadena, CA 91125 USA

[b]Department of Physics, Korea Advanced Institute of Science and Technology, Daejeon 305-701, Korea

ABSTRACT

Here, we emphasize the importance of a bottom reflector for achieving unidirectional far-field emission. As a result, over 80% of photons generated inside the cavity can be collected within a divergence angle of $\pm 30^\circ$ from the top. We also discuss interesting analogy in which the nanocavity-bottom reflector coupled system is treated as a point-like emitter in front of a mirror. Based on such a view point, the observed directivity is explained by using a comprehensive interference model. Finally, we propose a very practical form of an efficient photonic crystal nanolaser bonded on a flat metal surface, which may enable current injection and room-temperature continuous-wave operation.

Keywords: photonic crystal, FDTD, semiconductor laser, far-field, cavity quantum electrodynamics, single photon source, thresholdless laser

1. INTRODUCTION

Since the first demonstration of an optically pumped photonic crystal (PhC) slab nanocavity laser in 1999,[1] a two-dimensional (2-D) PhC slab structure became a vital platform for various PhC based photonic elements, such as waveguides and resonators. In particular, sub wavelength-scale cavities having high quality factors (Q) have drawn much attention due to their potential applications to high-efficiency single photon sources,[2,3] thresholdless lasers,[4] ultra high-speed modulation of semiconductor lasers,[5] and so on. There have been a plenty of improvements in the design of PhC nanocavities, including an electrically driven PhC nanolaser demonstrated in 2004, in which a submicron sized dielectric post was introduced as a current path.[6]

However, there still remain several critical drawbacks that should be addressed before applying such high Q/V cavities to real practical uses. Firstly, nanocavity based photon sources suffer from highly diffused far-field emission patterns, which seems to be inherent to their highly localized near-field patterns.[7] It should be noted that such poor directionality could not be resolved by operating the nanocavity as a laser and, therefore, the directionality is not an essential characteristic of nanolasers. Secondly, for most applications, one cannot avoid high heat generation rate within the nanocavity boundary. For example, in the case of air-suspended PhC slab nanolasers, a typical value of thermal resistance is known to be as high as 10^6 K/W, which hinders room-temperature (RT) continuous-wave (CW) operation of such nanolasers.[8,9] Finally, although there are already a few experimental reports addressing current injection nanolasers,[6] unique advantages enabled by the use of high Q/V, such as electrically driven ultra high-speed modulation > 100Gbit/s,[5] are yet to be demonstrated. Therefore, where and how to attach electrical contacts while maintaining high enough Q are still nontrivial open questions. Here, we would like to shed some light on those issues by proposing a novel design based on a bottom reflector.

Nanoengineering: Fabrication, Properties, Optics, and Devices VI, edited by Elizabeth A. Dobisz, Louay A. Eldada,
Proc. of SPIE Vol. 7402, 74020G · © 2009 SPIE · CCC code: 0277-786X/09/$18 · doi: 10.1117/12.826561

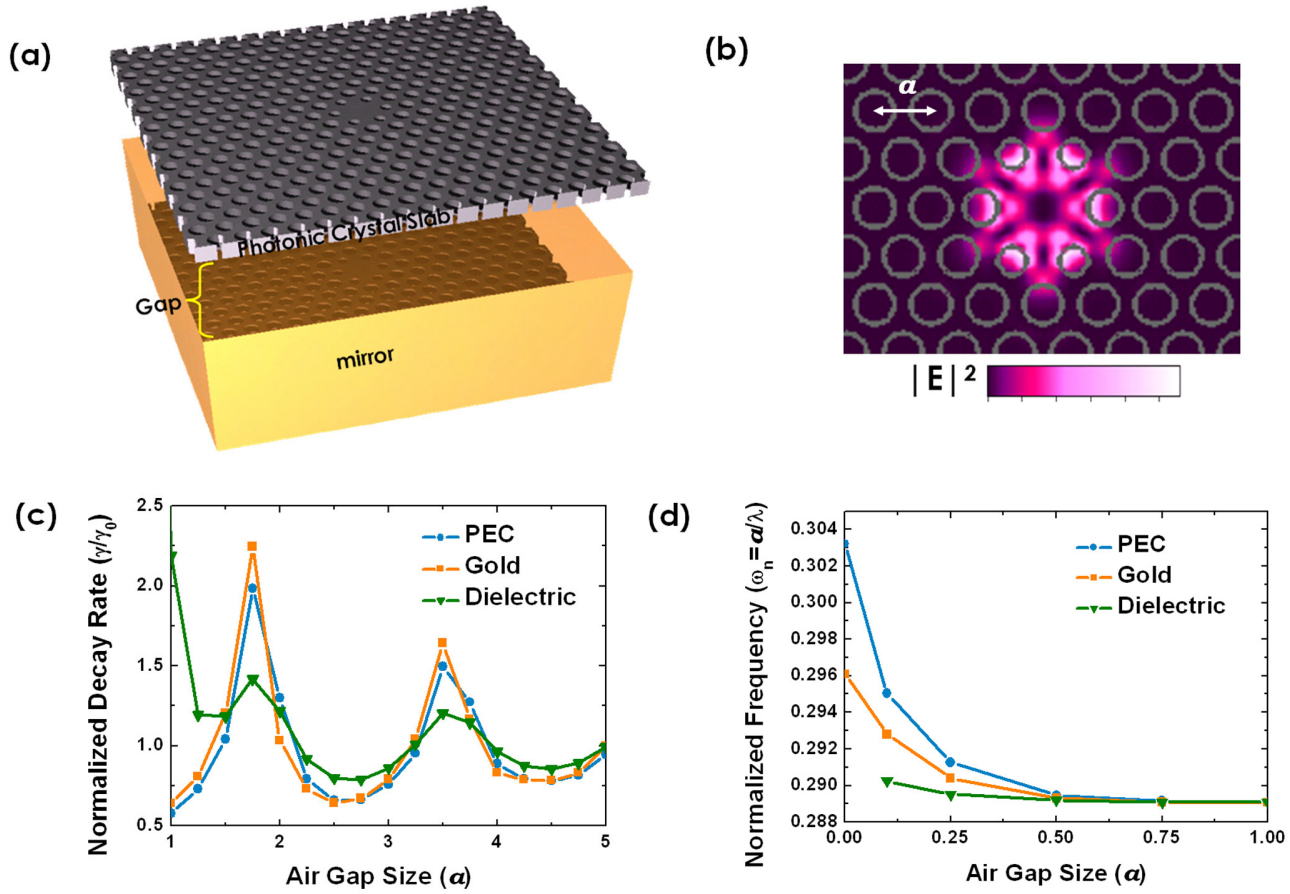

Figure 1. (a)A photonic crystal nanocavity is suspended in air in the vicinity of a bottom reflector. One can modify natural decay rate (γ_0) of the nanocavity mode by varying the air-gap size between the slab and the bottom reflector. (b) Electric-field intensity distribution ($|E|^2$) of the deformed hexapole mode detected in the middle of the slab. The lattice constant is denoted as 'a' throughout this paper. (c) Normalized decay rate of the nanocavity mode and (d) normalized resonant frequency of the nanocavity mode as a function of the air-gap size (in the unit of a). As a bottom reflector, three representative cases are considered; perfect electric conductor (PEC), gold, and dielectrics (of the same refractive index of 3.4 as the slab structure).

2. A PHOTONIC CRYSTAL NANOCAVITY NEARBY A BOTTOM REFLECTOR

Let us consider a PhC nanocavity placed nearby a bottom reflector, as depicted in Fig. 1(a). The present PhC nanocavity design (Fig. 1(b)) allows the deformed hexapole mode, whose Q is 15,000 in the absence of the reflector. As will be discussed, this situation is analogous to the well-known cavity quantum electrodynamics (cQED) example, a point dipole source near a perfect mirror. Clearly, Q of the nanocavity mode is much greater than that of a simple bottom reflector, which ensures the condition for the weak-coupling regime of cQED. Therefore, it is natural to expect to see similar enhancement or suppression of radiation rate and resultant modification of far-field emission profile in the nanocavity-reflector coupled system.

We have performed 3-D finite-difference time-domain (FDTD) simulation to study effects of the bottom reflector on the original radiation characteristics of the PhC nanocavity mode.[7] As we vary the air-gap size, Q factors can be estimated by time decaying behaviour of the cavity energy. Then, total decay rates of the PhC nanocavity mode (γ) are obtained through the relation of $\gamma = \omega/Q$, where ω is the angular frequency of the nanocavity mode.

In Fig. 1(c), we plot normalized decay rates for the deformed hexapole mode (γ/γ_0) as a function of the air-gap size, where γ_0 is the decay rate in the absence of the reflector. First, let us focus on the lossless perfect mirror (PEC). Clearly, the natural decay rate (γ_0) can be enhanced ($\gamma/\gamma_0 > 1$) or supressed ($\gamma/\gamma_0 < 1$) depending on the air-gap size. Note that, from Fig. 1(d), $1a$ is roughly equivalent to $0.29 \times \lambda$ when the cavity is sufficiently displaced from the mirror, where λ is the emission wavelength of the nanocavity mode in air. Thus, the distance between two consecutive peak positions (one at 1.75 a and the other at 3.5 a) is $\sim 0.5\lambda$, implying that interference associated with the air-gap size takes an important role in the observed modulation in the decay rate. It is also interesting to note that strongly enhanced decay rate or enhanced vertical emission (the equivalence between the two will be verified later) tends to occur when the air-gap size (d) satisfies $2d = m\lambda$, such as $d \sim 0.5\lambda$ and $d \sim 1.0\lambda$. As will be explained based on the planewave interference model, this condition is quite robust against the change in the PhC slab thicknesses. Now we consider more realistic material for a reflector, gold, whose optical constants are assumed for 1.3 μm. Slightly increased decay rates in the case of a gold mirror is partly due to light absorption in gold. Effect of the absorption in metal becomes more pronounced when $d < 0.5a$. If we replace the gold mirror with a simple dielectric interface, we get highly enhanced downward transmission through the bottom substrate, especially when $d < 1.2a$.[7] Finally, it is not surprising that the decay rate modulation weakens as a bottom mirror becomes less reflective.

To calculate the far-field pattern, we have used the 3-D FDTD method and the near- to far-field transformation algorithm.[7] All the far-field data (x, y) shown in this article are represented by using a simple mapping defined by $x = \theta \cos\phi$ and $y = \theta \sin\phi$. The refractive index of the PhC slab is chosen to be 3.4, which corresponds to that of InGaAsP around 1.3 μm. For real applications, one can insert active semiconductor layers, such as the InGaAsP quaternary quantum wells, in the middle of the slab. The air-hole radius and the slab thickness are chosen to be $0.35a$ and $0.90a$, respectively, where a represents the lattice constant of the triangular PhC.

In fact, for InP/InGaAsP material systems, one may utilize a flat surface of an InP substrate as a bottom reflector.[10,11] The refractive index contrast between InP and air is large enough to show interesting far-field interference results. Fig. 2 shows calculated far-field patterns of the deformed hexapole mode in the presence of a simple dielectric mirror, whose corresponding decay rates and resonant frequencies are shown in Fig. 1(c) and (d).

Firstly, one can clearly see the existence of concentric ring-type modulations laid upon the original far-field emission pattern (Fig. 2(a)), which is reminescent of the well known ring-type interference pattern from the Fabry-Perót etalon. Therefore, it is obvious that the interference between originally upward propagating wave and downward propagating wave is the key to understand the observed far-field emission patterns. Now, the role of the bottom reflector can be easily understood by this far-field interference. The downward-emitting photons will be redirected upward by the bottom reflector. It interferes with the originally upward-emitting photons. Secondly, one can either enhance or surpress the vertical emission by simply changing the air-gap size (d). Thirdly, one can get the more narrow and much more enhanced directional far-field emission pattern

For further information, contact Se-Heon Kim at seheon@caltech.edu

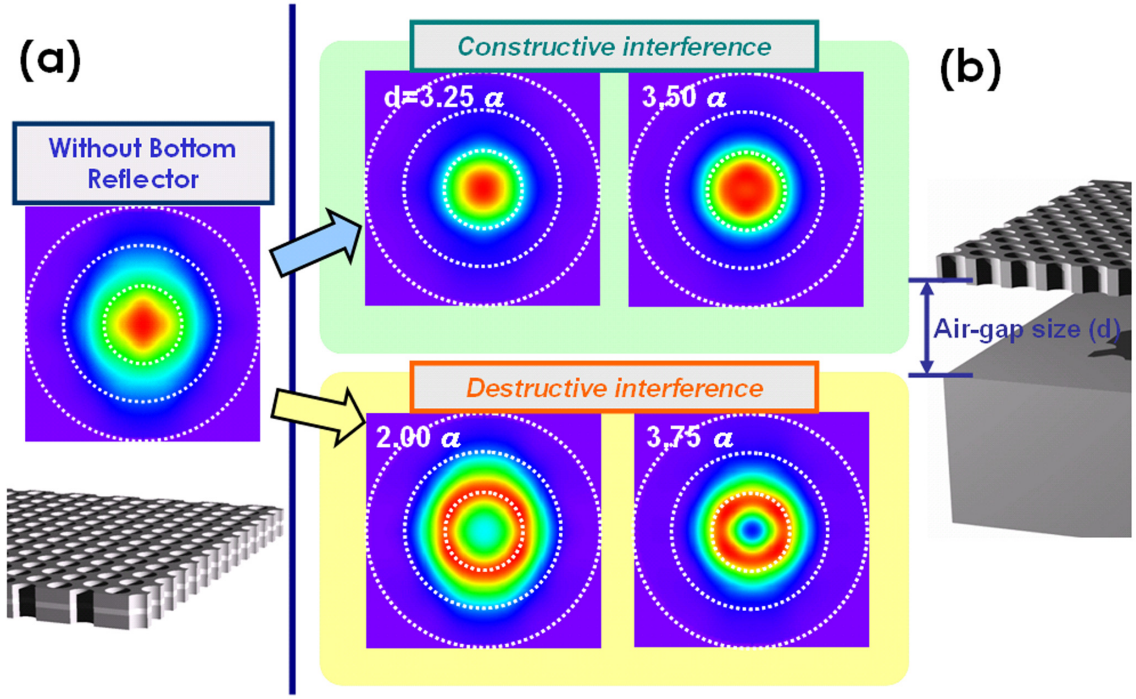

Figure 2. (a) Reference far-field emission pattern of the deformed hexapole mode in the absence of a bottom reflector. The PhC slab thickness is assumed to be 0.9 a. (b) Calculated far-field emission patterns of the deformed hexapole mode in the presence of a bottom reflector. Concentric ring type modulation of the original far-field pattern can clearly be seen. One can control the air-gap size to obtain either strongly enhanced or almost completely suppressed vertical emission. Here, a simple dielectric substrate is assumed as a bottom reflector. It should be noted that all the far-field data (x,y) are represented by using a simple mapping defined by $x = \theta\cos\phi$ and $y = \theta\sin\phi$ (the radius corresponds to θ).

compared with the reference emission pattern without having a bottom mirror. More quantitative analyses will be provided in the following section.

3. PLANEWAVE INTERFERENCE MODEL

To develop a simple and powerful model to explain all those features mentioned previously, firstly, we assume that the PhC slab can be approximated as a uniform dielectric slab having an effective refractive index.[12] Secondly, the PhC resonant mode that has modal volume of $\sim (\lambda/n)^3$ is treating as a point-like source located in the middle of the slab. Since we will consider only on-axis radiation ($\theta = 0$), all the emitted waves from the point-like source can, in fact, be described by scalar plane-waves. Thirdly, We assume that the bottom reflector is positioned sufficiently far ($> \lambda/2$) from the PhC slab so that the reflector does not perturb too much the original characteristics of the resonant mode. Thus, the initially upward and downward propagating waves can be assumed to be symmetric, 1 and 1.

Fig. 3(a) describes the situation where the emission from the cavity is divided by the upward and the downward propagating waves. r_0 and t_0 are coefficients of amplitude reflection and transmission for a single dielectric interface, respectively. Let S be the sum of all the waves detected upward which initially propagate downward. Then, an interference between the originally upward propagating wave and the S will be described by $1 + S$, and the resultant intensity will be proportional to $|1 + S|^2$. To sum all the waves which undergo infinitely many multiple reflections in the slab and in the air-gap, we used a simple method which takes advantage of the similarity of such multiple reflections and transmission processes. For further details on this calculation, please refer to the previous publication.[7] Here is the final result of the summation,

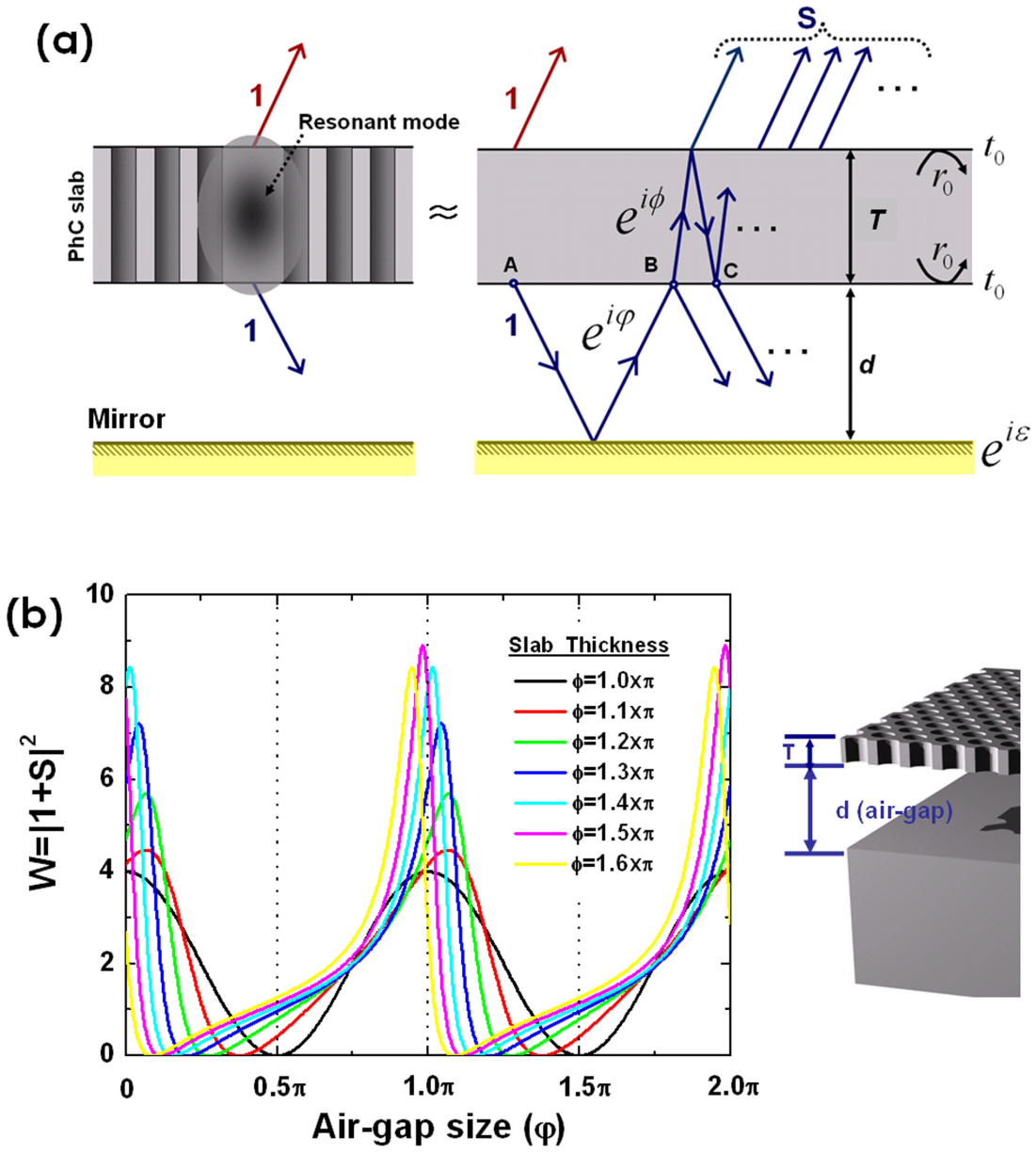

Figure 3. (a) Simple vertical interference model. The emission from the cavity is divided by the upward and the downward propagating waves. (b) Plots of vertical emission enhancement factors (W) obtained from the planewave interference model. Both the air-gap size and the slab thickness are varied, which are represented as phase thicknesses. Here, we have assumed the effective refractive index of the slab (n_{eff}) of 2.6, then $r_0 = (n_{eff} - 1)/(n_{eff} + 1) \approx 0.44$.

$$W = \left| 1 + \frac{t_0^2 e^{i\phi}}{(1 - r_0^2 e^{2i\phi})(r_0 - e^{-2i\varphi}) - r_0 t_0^2 e^{2i\phi}} \right|^2 . \quad (1)$$

Plots of W as a function of the air-gap size (φ) for several different slab thicknesses (ϕ) are summarized in Fig. 3(b). Now let's consider the case where the slab satisfies the 'slab resonance' condition, $\phi = 1.0\pi$. Since the slab becomes 'transparent' for any wave incident upon it, we get a simple two-beam interference result; W oscillates between 0 and 4. And the maximum enhancement of 4 is obtained when the air-gap thickness is an integral multiple of π.

Interesting phenomenon occurs when the slab thickness is made increase further than this 'slab resonance' condition. Now the slab is no longer transparent. As a result of multiple reflections and transmissions in the slab and the air-gap, the vertical enhancement factor can be greater than 4, the value that would result from the two-beam interference model. Moreover, there exists a broad acceptable range of air-gap sizes, that would give $W > 4$. Thus, experimental realization of such enhanced vertical beaming is rather robust against a possible deviation from the 1 λ air-gap.

Based on InGaAsP/InP material system, we recently demonstrated unidirectional PhC nanolasers emitting at near 1.55 μm.[11] The lasing action was obtained from the modified hexapole mode, whose emission characterisitics were modified by a simple flat InP substrate. The air-gap size was designed to be $\sim \lambda/2$ (actual thickness of the sacrificial layer = 860 nm). Although the InP substrate used here has only 30% reflectivity and the air-gap size is made 10% larger than the optimum thickness, fairly good directional far-field pattern has been obtained. It has been demonstrated that about 56% photons can funnell into a small divergence angle of $\pm 30^\circ$.

4. METAL-BONDED PHOTONIC CRYSTAL NANOCAVITY

According to the simple planewave interference model, the condition for air-gap size that gives well-directed vertical beaming is given as $2d = m\lambda$. Then, what would happen if we had zero air-gap which corresponds to the m=0 case? As shown in Fig. 1(c), when the bottom reflector is made of dielectric materials (e.g., simple dielectric substrate or DBR), cavity Q tends to decrease to zero as the air-gap size approaches to zero. However, one may find out some resonant modes that have large enough Q for actual lasing if the bottom reflector could be replaced by silver or gold, which is almost a perfect reflector at near infrared wavelengths. Figure 4(a) and (b) show numerically obtained electric-field intensity ($|E|^2$) and magnetic field (H_z) distributions, respectively, of the dipole mode in such a metal-bonded PhC nanocavity. This metal layer can provide highly efficient conduction pathways both for current and heat flows while it does not degrade the Q factor too much.

Furthermore, the flat metal surface can be used to enhance vertically emitted output power, enabling fairly good unidirectional vertical emission as presented in Fig. 4(b). Q factors in the range of $500 \sim 700$ are usually achievable by using gold. Further increase of the Q factor is expected by employing a thin-oxide layer positioned between the gold mirror and the PhC slab. We are currently working towards the realization of practical current injection nanolasers based on this metal-bonded structure and further details will be reported in our forthcoming papers. It should be note that the proposed vertical beaming scheme is not limited to this particular nanocavity geometry but may be applied to more general classes of nano- and micro-cavities, including plasmonic nanocavities, plasmon antennas, microdisks, and microspheres.

5. CONCLUSION

We have shown that inherent radiation properties of a PhC nanocavity mode, such as Q factors and far-field patterns, can be modified by placing a reflector nearby the cavity. To obtain uni-directional far-field emission, the air-gap size should be chosen as integral multiple of $\lambda/2$. Finally, we have proposed some of the very practical nanolaser designs based on a metal bonding technology, which may enable continuous current injection operation of PhC nanolasers at room-temperature.

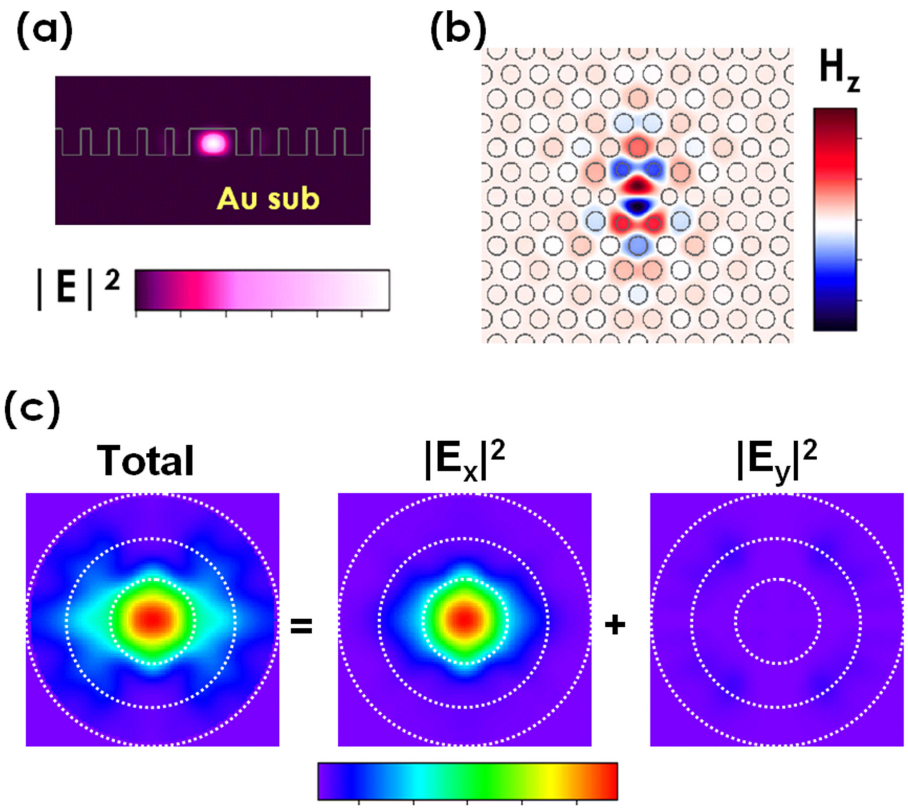

Figure 4. A photonic crystal nanocavity is brought in contact with a bottom reflector, which is assumed to be gold. Gold-bonded photonic crystal nanocavity may be considered as a special case of the zero air-gap in Fig. 1(a). (a) Electric-field intensity distribution ($|E|^2$) and (b) vertical component of magnetic-field distribution (H_z) in a gold-bonded photonic crystal nanocavity, where the lattice constant and the slab thickness are assumed to be 340 nm and 350 nm, respectively, which results in emission wavelength of $\sim$ 1316 nm and cavity Q factor of $\sim$ 600. (c) By optimizing the slab thickness, linearly-polarized, unidirectional far-field emission can be obtained.

ACKNOWLEDGMENTS

This work was supported in part by the Air Force Office of Scientific Research (FA9550-04-1-0434), the Army Research Office (W911NF-07-1-0277), and the National Science Foundation (EEC-0812072). We gratefully acknowledge critical support and infrastructure provided for this work by the Kavli Nanoscience Institute at Caltech.

REFERENCES

[1] O. Painter, R. K. Lee, A. Yariv, A. Scherer, J. D. O'Brien, P. D. Dapkus, and I. Kim, "Two-dimensional photonic band-gap defect mode laser," *Science* **284**, 1819–1821 (1999).

[2] Se-Heon Kim, Sun-Kyung Kim, and Yong-Hee Lee, "Toward efficient unidirectional photonic crystal light emitters," *Proc. SPIE* **6352**, 635213 (2006).

[3] I. Friedler, C. Sauvan, J. P. Hugonin, P. Lalanne, J. Claudon, and J. M. Gerard, "Solid-state single photon sources: the nanowire antenna," *Opt. Express* **17**, 2095–2110 (2009).

[4] Yokoyama, H., "Physics and Device Applications of Optical Microcavities," *Science* **256**, 66–70 (1992).

[5] Hatice Altug, Dirk Englund, and Jelena Vukovic, "Ultrafast photonic crystal nanocavity laser," *Nat. Phys.* **2**, 484–488 (2006).

[6] Hong-Gyu Park, Se-Heon Kim, Soon-Hong Kwon, Young-Gu Ju, Jin-Kyu Yang, Jong-Hwa Beak, Sung-Bock Kim, and Yong-Hee Lee, "Electrically Driven Single-Cell Photonic Crystal Laser," *Science* **305**(5689), 1444–1447 (2004).

[7] S. H. Kim, S. K. Kim, and Y. H. Lee, "Vertical beaming of wavelength-scale photonic crystal resonators," *Phys. Rev. B* **73**, 235117 (2006).

[8] Kengo Nozaki, Shota Kita, and Toshihiko Baba, "Room temperature continuous wave operation and controlled spontaneous emission in ultrasmall photonic crystal nanolaser," *Opt. Express* **15**, 7506–7514 (2007).

[9] Se-Heon Kim, Jae-Hoon Choi, Seung-Kon Lee, Shin-Hyun Kim, Seung-Man Yang, Yong-Hee Lee, Christian Seassal, Philippe Regrency, and Pierre Viktorovitch, "Optofluidic integration of a photonic crystal nanolaser," *Opt. Express* **16**, 6515–6527 (2008).

[10] Se-Heon Kim, Min-Kyo Seo, Ju-Young Kim, and Yong-Hee Lee, "Effects of a bottom substrate on emission properties of a photonic crystal nanolaser," *Indium Phosphide & Related Materials, 2007, IEEE* **17**, 480–483 (2007).

[11] Ju-Hyung Kang, Min-Kyo Seo, Sun-Kyung Kim, Se-Heon Kim, Myung-Ki Kim, Hong-Gyu Park, Ki-Soo Kim, and Yong-Hee Lee, "Polarized vertical beaming of an engineeredhexapole mode laser," *Opt. Express* **17**, 6074–6081 (2009).

[12] S. Fan and J. D. Joannopoulos, "Analysis of guided resonances in photonic crystal slabs," *Phys. Rev. B* **65**, 235112 (2002).